Research Article Vol. 30, No. 9 / 25 Apr 2022 / Optics Express 14553
Optics EXPRESS

Channeled spectropolarimeter with arbitrary retarder orientation settings

PENGHUI LIU,[1,2] XUEPING JU,[1,*] BIN YANG,[3] CHANGXIANG YAN,[1,4] TAO ZHANG,[1,2,4] GUOHAO JU,[1] AND WENHE XING[1]

[1] *Changchun Institute of Optics, Fine Mechanics and Physics, Chinese Academy of Sciences, Changchun 130033, China*
[2] *University of Chinese Academy of Sciences, Beijing 100049, China*
[3] *Yusense Information Technology and Equipment (Qingdao) Inc., Qingdao 266000, China*
[4] *Center of Materials Science and Optoelectrics Engineering, University of Chinese Academy of Science, Beijing 100049, China*
[*] *juxueping@ciomp.ac.cn*

Abstract: A channeled spectropolarimeter can simultaneously obtain intensity, spectral, and polarization information. In the traditional model, the retarders must be oriented at specific angles. However, misalignments of the retarders are inevitable during assembly, and the status of the retarders is sensitive to environmental perturbations, which affects the performance of the channeled spectropolarimeter. In this study, a general channeled spectropolarimeter model was derived, in which the retarder orientations can be arbitrary and unknown. Meanwhile, the system is unaffected by environmental perturbation because it can self-calibrate to avoid fluctuations in the retarder orientations and phase retardations. The effectiveness and robustness of the model were verified through simulations and experiments.

1. Introduction

Spectropolarimetry quantifies both the polarization state and spectral content of light, which is significance in many fields, such as remote sensing [1–3], biomedicine [4–6], and environmental monitoring [7]. Among the various spectropolarimeter instruments developed in the past, channeled spectropolarimetry (CSP), proposed by Oka et al. [8] and Iannarilli et al. [9], is a powerful snapshot technique. It utilizes two high-order retarders and a linear polarizer to achieve polarimetric spectral intensity modulation (PSIM) in the wavenumber domain. The Stokes parameters are separated in the optical path difference (OPD) domain channels, which can be reconstructed using Fourier transform and frequency-filtering techniques. Furthermore, it has a simple optical system with no mechanically movable components. Therefore, it has great potential for practical applications.

Conventional CSP system requires the fast axes of the two retarders to be oriented at 0° and 45°. However, alignment errors are inevitable during the assembly [10]. Different combinations of alignment errors result in different errors in the reconstructed Stokes parameters. In addition, the phase retardations of the two retarders may differ from those calibrated in the laboratory owing to environmental perturbations, such as temperature fluctuations [11], causing the reconstructed Stokes parameters to deviate from their true values. Furthermore, the performance of the CSP system will also degrade if it is used on a vibration platform [12–15], such as in spaceborne and airborne applications, and it is quite difficult to recalibrate it for spaceborne systems because of its high cost.

Mu et al. [10] used two linearly polarized beams oriented at 22.5° and 45° to calibrate the orientation errors of the fast axes of high-order retarders with different signs. Yang et al. [16] used an additional high-order retarder to determine the alignment errors and compensate for them. Ju et al. [17] proposed a modified reference beam calibration technique that employ the

#456437 https://doi.org/10.1364/OE.456437
Journal © 2022 Received 16 Feb 2022; revised 20 Mar 2022; accepted 21 Mar 2022; published 18 Apr 2022

Optics EXPRESS

amplitude terms and simplifies the calibration process [18]. Sabatke et al. [19,20] modeled the CSP as a linear operator for calibration, and Zhou et al. [21] significantly reduced the measurement times. These methods solve alignment errors that may occur during assembly and adjustment in the laboratory. For the phase fluctuations of high-order retarders caused by the environmental perturbations, Taniguchi and Oka [22] proposed a self-calibration method when there are no alignment errors, while Xing et al. [23] considered both environmental perturbations and alignment errors. However, these methods are based on specific retarder orientations, which limits the potential of CSP.

We eliminated the requirement for specific retarder orientations. The retarder orientations can be arbitrary and unknown, according to the principle of CSP; from this perspective, there is no alignment errors. Furthermore, we found that the CSP has the potential for self-calibration in all cases and can be immune to retarder orientations and retardation changes caused by platform vibrations and environmental perturbations. By using the new model, the limitations of the CSP can be significantly reduced, and tolerance requirements during assembly can be greatly relaxed.

The remainder of this paper is organized as follows: Section 2 provides the principle of the general CSP with arbitrary retarder orientations. The simulation and experimental verification are presented in Sections 3 and 4, respectively. Finally, Section 5 concludes the study.

2. Theory

In this section, we derive a model for arbitrary retarder orientation settings of the CSP system. The retardations and orientations of the retarders were determined using two methods: laboratory calibration and self-calibration.

2.1. Principle of the general channeled spectropolarimetry

An optical schematic of the CSP is shown in [Fig. 1]. It was composed of two thick retarders (R_1 and R_2) and a polarizer (A). The fast axes of R_1 and R_2 form angles α and β, respectively, with the transmission direction of A. Given that A is the benchmark for the system to work with the spectrometer, we set it to 0° for simplicity. Note that $\alpha = \beta$, $\alpha = \beta + 90°$, $\beta = 0°$, and $\beta = 90°$ are not allowed due to the principle of CSP.

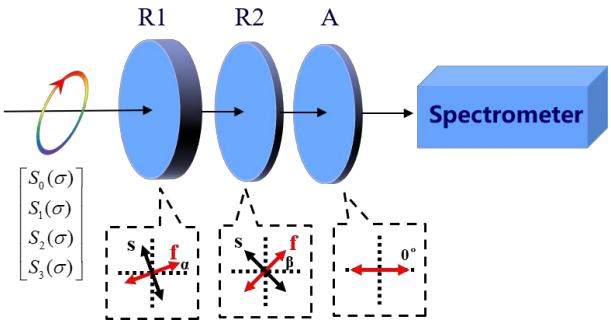

Fig. 1. Schematic of the general channeled spectropolarimeter.

Optics EXPRESS

The Muller matrices of R_1, R_2, and A are

$$M_{R_1}(\alpha,\phi_1)=\begin{bmatrix}1 & 0 & 0 & 0\\ 0 & b^2+a^2\cos\phi_1 & ab(1-\cos\phi_1) & -a\sin\phi_1\\ 0 & ab(1-\cos\phi_1) & a^2+b^2\cos\phi_1 & b\sin\phi_1\\ 0 & a\sin\phi_1 & -b\sin\phi_1 & \cos\phi_1\end{bmatrix}, \tag{1}$$

$$M_{R_2}(\beta,\phi_2)=\begin{bmatrix}1 & 0 & 0 & 0\\ 0 & d^2+c^2\cos\phi_2 & cd(1-\cos\phi_2) & -c\sin\phi_2\\ 0 & cd(1-\cos\phi_2) & c^2+d^2\cos\phi_2 & d\sin\phi_2\\ 0 & c\sin\phi_2 & -d\sin\phi_2 & \cos\phi_2\end{bmatrix}, \tag{2}$$

$$M_A(0^\circ)=\frac{1}{2}\begin{bmatrix}1 & 1 & 0 & 0\\ 1 & 1 & 0 & 0\\ 0 & 0 & 0 & 0\\ 0 & 0 & 0 & 0\end{bmatrix}, \tag{3}$$

where $a=\sin(2\alpha)$, $b=\cos(2\alpha)$, $c=\sin(2\beta)$, and $d=\cos(2\beta)$. ϕ_1 and ϕ_2 represent the phase retardations of R_1 and R_2, respectively. The spectrum obtained by the spectrometer is expressed as

$$\begin{aligned}
I(\sigma) &= M_A(0^\circ)\cdot M_{R_2}(\beta,\phi_2)\cdot M_{R_1}(\alpha,\phi_1)\cdot S_{in}\\
&= \frac{1}{2}[S_0+b^2d^2S_1+abcdS_1+abd^2S_2+a^2cdS_2]\\
&+\frac{1}{4}[b^2c^2S_1-abcdS_1+abc^2S_2-a^2cdS_2]\exp(i\phi_2)\\
&+\frac{1}{4}[b^2c^2S_1-abcdS_1+abc^2S_2-a^2cdS_2]\exp(-i\phi_2)\\
&+\frac{1}{8}[a^2c^2S_1+abcdS_1-acS_1-abc^2S_2-b^2cdS_2+bcS_2+iac^2S_3+ibcdS_3-icS_3]\exp[i(\phi_1-\phi_2)]\\
&+\frac{1}{8}[a^2c^2S_1+abcdS_1-acS_1-abc^2S_2-b^2cdS_2+bcS_2+iac^2S_3-ibcdS_3+icS_3]\exp[-i(\phi_1-\phi_2)]\\
&+\frac{1}{4}[a^2d^2S_1-abcdS_1-abd^2S_2+b^2cdS_2+iad^2S_3-ibcdS_3]\exp(i\phi_1)\\
&+\frac{1}{4}[a^2d^2S_1-abcdS_1-abd^2S_2+b^2cdS_2-iad^2S_3+ibcdS_3]\exp(-i\phi_1)\\
&+\frac{1}{8}[a^2c^2S_1+abcdS_1+acS_1-abc^2S_2-b^2cdS_2-bcS_2+iac^2S_3+ibcdS_3+icS_3]\exp[i(\phi_1+\phi_2)]\\
&+\frac{1}{8}[a^2c^2S_1+abcdS_1+acS_1-abc^2S_2-b^2cdS_2-bcS_2+iac^2S_3-ibcdS_3-icS_3]\exp[-i(\phi_1+\phi_2)],
\end{aligned} \tag{4}$$

where the wavenumber dependence was ignored for simplicity. Using the inverse Fourier transform to calculate the autocorrelation function of I(σ), we can obtain nine channels containing different polarization information:

$$\begin{aligned}
C(L) &= C_0(L)+C_1(L-L_2)+C_{-1}(L+L_2)\\
&+C_2(L-(L_1-L_2))+C_{-2}(L+(L_1-L_2))\\
&+C_3(L-L_1)+C_{-3}(L+L_1)\\
&+C_4(L-(L_1+L_2))+C_{-4}(L+(L_1+L_2)),
\end{aligned} \tag{5}$$

where

$$C_0=F^{-1}\{\frac{1}{2}[S_0(\sigma)+dfS_{12}(\sigma)]\}, \tag{6a}$$

Optics EXPRESS

$$C_1 = F^{-1}\{\frac{1}{4}ceS_{12}(\sigma)\exp(i\phi_2)\}, \tag{6b}$$

$$C_{-1} = F^{-1}\{\frac{1}{4}ceS_{12}(\sigma)\exp(-i\phi_2)\}, \tag{6c}$$

$$C_2 = F^{-1}\{\frac{1}{8}c(f-1)S_{123}(\sigma)\exp[i(\phi_1-\phi_2)]\}, \tag{6d}$$

$$C_{-2} = F^{-1}\{\frac{1}{8}c(f-1)S^*_{123}(\sigma)\exp[-i(\phi_1-\phi_2)]\}, \tag{6e}$$

$$C_3 = F^{-1}\{-\frac{1}{4}deS_{123}(\sigma)\exp(i\phi_1)\}, \tag{6f}$$

$$C_{-3} = F^{-1}\{-\frac{1}{4}deS^*_{123}(\sigma)\exp(-i\phi_1)\}, \tag{6g}$$

$$C_4 = F^{-1}\{\frac{1}{8}c(f+1)S_{123}(\sigma)\exp[i(\phi_1+\phi_2)]\}, \tag{6h}$$

$$C_{-4} = F^{-1}\{\frac{1}{8}c(f+1)S^*_{123}(\sigma)\exp[-i(\phi_1+\phi_2)]\}, \tag{6i}$$

and

$$\begin{cases} e = bc - ad = \sin 2(\beta-\alpha) \\ f = ac + bd = \cos 2(\beta-\alpha) \end{cases}, \tag{7}$$

$$\begin{cases} S_{12}(\sigma) = bS_1(\sigma) + aS_2(\sigma) \\ S_{123}(\sigma) = aS_1(\sigma) - bS_2(\sigma) + iS_3(\sigma) \end{cases}. \tag{8}$$

To make full use of the information of the nine channels, an appropriate thickness ratio of R_1 to R_2 must be satisfied to avoid overlap between the channels. In this study, we used a thickness ratio of 3:1; thus, C_{-4}–C_4 were uniformly distributed in the optical-path difference domain. Using frequency filtering and Fourier transform, the Stokes parameters can be reconstructed as

$$S_0 = 2F(C_0) - dfS_{12}(\sigma), \tag{9a}$$

$$S_1 = bS_{12}(\sigma) + a\mathrm{Re}[S_{123}(\sigma)], \tag{9b}$$

$$S_2 = aS_{12}(\sigma) - b\mathrm{Re}[S_{123}(\sigma)], \tag{9c}$$

$$S_3 = \mathrm{Im}[S_{123}(\sigma)], \tag{9d}$$

where

$$\begin{cases} S_{12}(\sigma) = \frac{4F(C_1)}{ce\cdot\exp(i\phi_2)} \\ S_{123}(\sigma) = \frac{8F(C_4)}{c(f+1)\cdot\exp[i(\phi_1+\phi_2)]} \end{cases}. \tag{10}$$

The Stokes parameters can be reconstructed as long as the phase retardations and retarder orientations are known.

Optics EXPRESS

2.2. Calibrate the phase retardations

The instrument usually needs to be calibrated in the laboratory before practical application. To calibrate the phase retardations of R_1 and R_2 in the laboratory, we used a linearly polarized light oriented at an arbitrary angle θ, whose Stokes vector can be expressed as

$$S_{LP,\theta}(\sigma) = S_0^{\theta}(\sigma) \cdot [\ 1 \quad \cos(2\theta) \quad \sin(2\theta) \quad 0\ ]^T, \tag{11}$$

where $S_{LP,\theta}(\sigma)$ and $S_0^{\theta}(\sigma)$ denote Stokes vector and the first parameter in the vector. When it passes through the CSP system, the content in the desired channel is expressed as

$$C_3' = F^{-1}\{-\frac{1}{4}deS_{123}'(\sigma)\exp(i\phi_1)\}, \tag{12}$$

$$C_4' = F^{-1}\{\frac{1}{8}c(f+1)S_{123}'(\sigma)\exp[i(\phi_1+\phi_2)]\}, \tag{13}$$

where

$$S_{123}'(\sigma) = S_0^{\theta}(\sigma)\sin 2(\alpha-\theta). \tag{14}$$

If the angle of the linearly polarized light is not parallel to the axis of R_1, that is, $S'_{123}(\sigma) \neq 0$, ϕ_1, and ϕ_2 can be obtained by taking the arguments of C_3' and C_4'/C_3', respectively.

Because high-order retarders are used in CSP system, even though the phase retardations are accurately calibrated in the laboratory, they are still susceptible to environmental perturbations, such as temperature changes during applications [23], thereby degrading the performance of the instrument. Therefore, the phase retardations must be calibrated in real time. Fortunately, we found that CSP inherently possesses the ability to self-calibrate under all circumstances. Since $f^2 + e^2 = 1$, from [Eq. (8)], we find that

$$S_{12}^2(\sigma) + |S_{123}(\sigma)|^2 = S_1^2(\sigma) + S_2^2(\sigma) + S_3^2(\sigma), \tag{15}$$

where $|\cdot|$ stands for the operator to take the modulus. Therefore, we obtain

$$16[F(C_1)]^2 - 64F(C_2)F(C_{-4}) = c^2e^2[S_1^2(\sigma) + S_2^2(\sigma) + S_3^2(\sigma)]\exp(2i\phi_2). \tag{16}$$

This equation is similar to that proposed by Taniguchi and Oka [18]. It is easy to show that both c^2 and e^2 are greater than 0, if the principle of CSP is followed. Therefore, ϕ_2 can be obtained by taking the argument of [Eq. (16)], regardless of the state of polarization (SOP) of the incident light. The other phase retardation ϕ_1 can be obtained using ϕ_2 and the thickness ratio of R_1 and R_2, as the two retarders are compact and undergo the same environmental perturbations.

It should be noted that the phases obtained using [Eq. (16)] is $2\phi_2$, which belongs to $(-\pi, \pi)$. Phase ambiguity may occur when calculating ϕ_2. To avoid this, an appropriate reference wavenumber must be chosen for phase unwrapping and it should be compared with the phase calibrated in the laboratory. In addition, phase ambiguity may also be caused by temperature changes, which has been addressed by Chrysler et al. [24]; therefore, this is not our focus.

2.3. Determine the retarder orientations

To determine the orientations of the retarders, we must determine the quadrants of α and β to avoid sign errors before determining their values. In practical applications, the values of α and β are set artificially before adjustment. Commercial retarders generally indicate the direction of the fast axis, and laboratories usually have precision adjustment devices; therefore, the first step can be skipped. However, to improve the applicability of the proposed model and avoid a situation where the fast axis direction is not indicated on the retarders, we still introduce a method to determine the quadrants of α and β.

Optics EXPRESS

2.3.1. Determining the quadrants of α and β

Three reference beams were used to determine the quadrants of α and β: two linearly polarized beams oriented at 0° and 45°, and one circularly polarized beam. First, the circularly polarized light was used for calibration, where the content of the desired channel is

$$C_{2,\text{circular}} = F^{-1}\{\frac{1}{8}c(f-1)S_{3,\text{circular}}(\sigma)\exp[i(\phi_1-\phi_2)]\}, \tag{17}$$

$$C_{4,\text{circular}} = F^{-1}\{\frac{1}{8}c(f+1)S_{3,\text{circular}}(\sigma)\exp[i(\phi_1+\phi_2)]\}, \tag{18}$$

where ϕ_1 and ϕ_2 are determined in Subsection 2.2, and thus, f can be calculated as

$$f = \frac{\frac{C_{4,\text{circular}}}{C_{2,\text{circular}}}\exp(-2i\phi_2)+1}{\frac{C_{4,\text{circular}}}{C_{2,\text{circular}}}\exp(-2i\phi_2)-1}. \tag{19}$$

Because the f from the above equation has the correct value and sign, the sign of c can be obtained from $C_{4,\text{circular}}/\exp[i(\phi_1+\phi_2)]$. It should be noted that here we only need to know the sign of $S_{3,\text{circular}}$, so the result will not be affected even if there is small error in $S_{3,\text{circular}}$. Then, we use 0° linearly polarized light for calibration, and the content in the desired channel is expressed as

$$C_{2,0^\circ} = F^{-1}\{\frac{1}{8}ac(f-1)S_{0,0^\circ}(\sigma)\exp[i(\phi_1+\phi_2)]\}, \tag{20}$$

where the signs of $S_{0,0^\circ}$, c, and (f-1) are known, and the exponential term has been determined. Thus, the sign of a can be obtained from the above equation. Finally, we used a beam of 45° linearly polarized light for calibration, and the contents in the desired channels were

$$C_{1,45^\circ} = F^{-1}\{\frac{1}{4}ceaS_{0,45^\circ}(\sigma)\exp(i\phi_2)\}, \tag{21}$$

$$C_{2,45^\circ} = F^{-1}\{\frac{1}{8}bc(1-f)S_{0,45^\circ}(\sigma)\exp[i(\phi_1-\phi_2)]\}, \tag{22}$$

$$C_{3,45^\circ} = F^{-1}\{\frac{1}{4}debS_{0,45^\circ}(\sigma)\exp(i\phi_1)\}. \tag{23}$$

The signs of e, b, and d can be determined sequentially using [Eqs. (21)–(23)]. Once the signs of a–f are determined, the quadrants of α and β can be determined.

2.3.2. Determine the values of α and β

After determining the ranges of α and β, their values were calculated, and using [Eqs. (6.a)–(6.i)] we obtain

$$\frac{F(C_4)}{F(C_2)} = \frac{f+1}{f-1}\exp(2i\phi_2), \tag{24}$$

$$\frac{F(C_3)}{F(C_4)} = \frac{-2de}{c(f+1)}\exp(-i\phi_2). \tag{25}$$

With [Eqs. (24)–(25)] and $f^2+e^2=1$, the retarder orientations can be obtained as follows:

$$f = \frac{\frac{F(C_4)}{F(C_2)}\exp(-2i\phi_2)+1}{\frac{F(C_4)}{F(C_2)}\exp(-2i\phi_2)-1}, \tag{26}$$

$$\frac{d}{c} = -\frac{f+1}{e}\frac{F(C_3)}{2F(C_4)}\exp(i\phi_2). \tag{27}$$

Optics EXPRESS

Note that $d/c = \cot 2\beta$, then α and β are given as

$$\alpha = -\frac{1}{2}\arccos(f) + \frac{1}{2}\mathrm{arccot}(\frac{d}{c}), \tag{28}$$

$$\beta = \frac{1}{2}\mathrm{arccot}(\frac{d}{c}). \tag{29}$$

Once α and β have been determined, the Stokes parameters can be reconstructed according to [Eqs. (9a)–(9d)].

In particular, if none of channels C_2–C_4 exist, that is $S_{123} = 0$. This means that the target light is linearly polarized, assuming that it has an orientation of γ, from [Eq. (8)], we obtain

$$\begin{cases} S''_{123} = \sin 2(\alpha - \gamma) = 0 \\ S''_{12} = \cos 2(\alpha - \gamma) \end{cases}. \tag{30}$$

Therefore, $\gamma = \alpha$ ($S_{12} = 1$), or $\gamma = \alpha + 90°$ ($S_{12} = -1$), which means that the incident light is linearly polarized parallel to the fast axis ($S_{12} = 1$) or slow axis ($S_{12} = -1$) of R_1. Because the signs of c and e are known, the sign of S_{12} can be obtained using the sign of $C_1 / \exp(i\phi_2)$. Conversely, the target light is linearly polarized at an angle of 45° to the axis of R_1 if C_1 channel does not exist.

Using the established model, the Stokes parameters can be accurately reconstructed when the retarder orientations are arbitrary, and there is a change in temperature.

3. Simulation analysis

The effectiveness of the proposed model was verified via a simulation. The wavenumber range in the simulation was 12,000–17143 cm-1 (583–833 nm). The thicknesses of R_1 and R_2 were 6 and 2 mm, respectively. The retarders were made of quartz, whose birefringence can be obtained from [25]. We used a 30° linearly polarized beam as the target light, and the orientations of R_1 and R_2 were arbitrarily set to 20° and 70°, respectively, for the demonstration.

[Fig. 2] shows the magnitude of the autocorrelation function. As expected, nine channels were separated. The calculation results for the retarder orientations are shown in [Fig. 3]. Because the retarder orientations are independent of the wavenumber, we use the average value under different wavenumbers as the final results, which are shown in Table 1. These results suggest that the retarder orientations can be accurately determined using the proposed method, which lays the foundation for reconstructing Stokes parameters.

Table 1. Averages and errors of the calculated results of α and β

Parameter	Input value	Calculated value	Error
α	20°	20.0222°	0.0222°
β	70°	70.0347°	0.0347°

The results of the reconstructed Stokes parameters are shown in [Fig. 4]. Using the presented method, the residual errors of S_1/S_0 and S_2/S_0 and S_3/S_0 are 1.94×10^{-4} and 8.77×10^{-5} and 2.07×10^{-4}, respectively; the residual error of the degree of polarization (DOP) is 2.95×10^{-4}. These results indicate that the calibration and reconstruction methods are effective.

To further verify the performance of the proposed model and to demonstrate its generality, we set the input light to $S_1(\sigma) = S_2(\sigma) = S_3(\sigma) = S_0(\sigma)/\sqrt{3}$ and traversed all possible values of α and β from 1° to 180°. The residual errors of DOP are shown in [Fig. 5]. The white part in the figure represents the cases that does not conform to the principle of CSP, corresponding to $\alpha = \beta$,

Optics EXPRESS

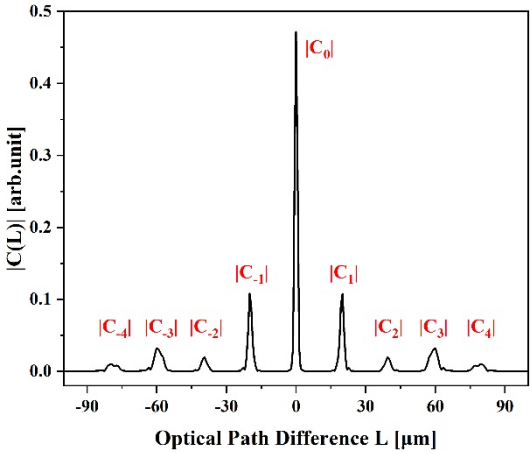

Fig. 2. The magnitude of the autocorrelation function of the modulated spectrum.

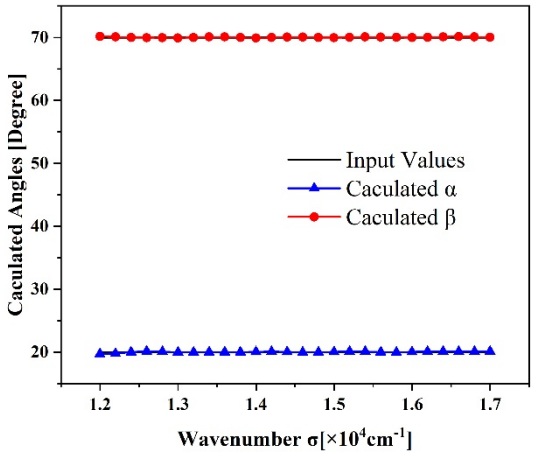

Fig. 3. Calculated results of the azimuth angles of R_1 and R_2.

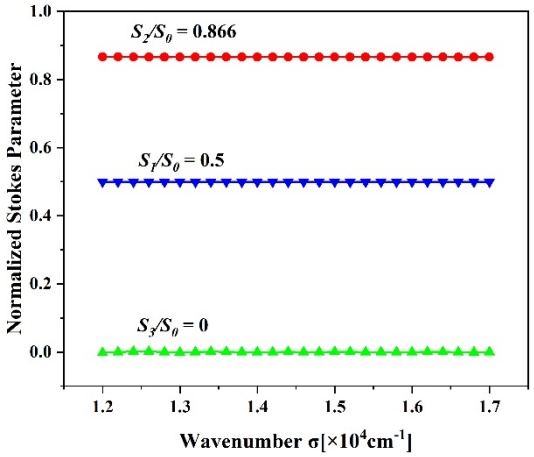

Fig. 4. Reconstructed results of Normalized Stokes Parameters, theoretical values are $S_1/S_0 = 0.5$, $S_2/S_0 = 0.866$, and $S_3/S_0 = 0$.

Optics EXPRESS

$\alpha = \beta + 90°$, $\beta = 0°$, and $\beta = 90°$. [Figure 5] shows that the reconstruction accuracy was better when the fast axes of R_1 and R_2 were in the same quadrant. In addition, the closer the axes of R_2 are to the transmission axis of A, the further the axes of R_1 must be separated from the axes of R_2. When β is in the range of 30°–70°, the fast axis of R_1 only needs to be separated from the fast axis of R_2 by 2° to ensure accuracy. However, if the angle between the fast axis of R_2 and the transmission axis of A is less than 10°, then the fast axis of R_1 is preferably separated from the fast axis of R_2 by more than 10°. This is because the coefficients of the channels are too small, making them more susceptible to crosstalk.

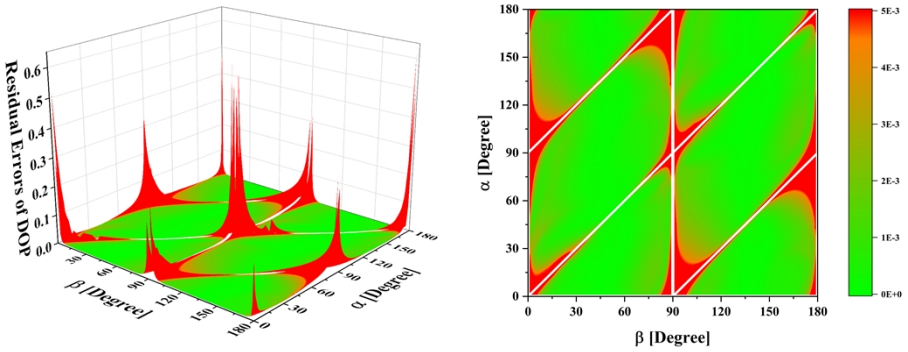

Fig. 5. Residual errors of reconstructed results of DOP at all possible orientation combinations.

It should be noted that we used the same rectangular window for filtering in all cases in the simulation. The red part is smaller if the filter window is modified accordingly. Therefore, even if the residual DOP errors at some points in [Fig. 5] are of the order of 10^{-3}, such as $\alpha = 16°$and $\beta = 6°$, the CSP still has sufficient accuracy in this case, which is verified in the experiments in the next section.

The simulation results suggest that the presented model is very robust, the orientations of R_1 and R_2 can be accurately calculated, and the Stokes parameters can be accurately reconstructed. In addition, the tolerance requirements for assembly and adjustment have been drastically relaxed, which is of great significance for the development of the instrument.

4. Experimental results

The feasibility of the proposed model was demonstrated using the experimental setup shown in [Fig. 6]. It consists of a polarizer, two retarders with the same thickness and material as in the simulation, and a spectrometer (ASD FieldSpec 3). A stabilized tungsten halogen lamp, collimator, and rotatable polarizer P, were used to generate the target beams. The wavenumber range was consistent with the simulation settings.

Because the angle between the fast axes of the two retarders is in the range of 0°–90°, we set four different combinations of α and β with differences of 10°, 30°, 50°, and 70°. To verify the self-calibration capability of the CSP system, we changed the temperature from 21 °C to 27 °C to change the retardations. The measured results at $\alpha = 20°$ and $\beta = 70°$ are shown in [Fig. 7]. The desired channels were separated from one another, and their distributions were consistent with the simulation results, which further validated the proposed model.

The reconstructed Stokes parameters for these cases are shown in [Fig. 8(a)], and [Fig. 8(b)] gives the reconstructed Stokes parameters at different temperatures when $\alpha = 20°$ and $\beta = 70°$. Notably, the normalized Stokes parameters under different orientation settings almost overlap with each other. The residual errors of S_1/S_0, S_2/S_0, and S_3/S_0 were less than 5.9×10^{-3}, 5.6×10^{-3}, and 6.6×10^{-3}, respectively. The residual errors of the DOP were less than 4.1×10^{-3}, which

Optics EXPRESS

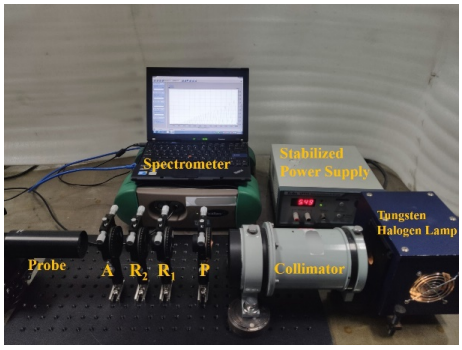

Fig. 6. Experimental setup.

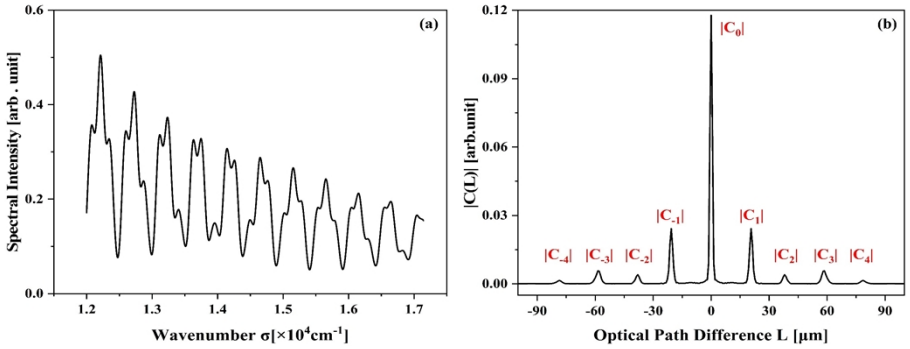

Fig. 7. Measured results (a) Measured spectral intensity; (b) Magnitude of the autocorrelation function of the modulated spectrum.

meets practical application requirements [26]. Owing to the self-calibration capability of the system, the reconstructed Stokes parameters were hardly affected by the temperature changes.

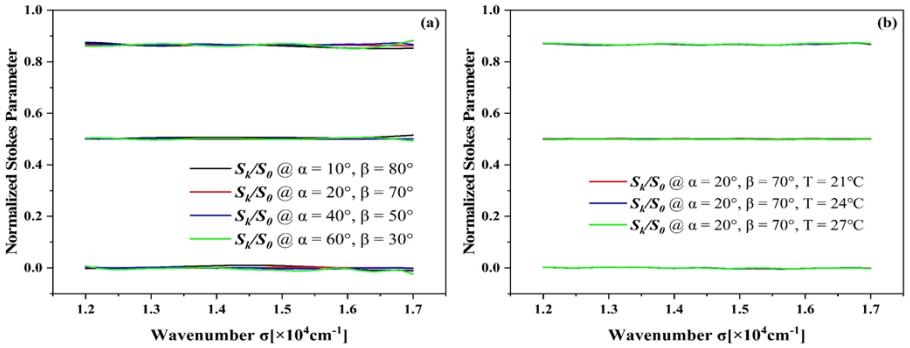

Fig. 8. Reconstructed Stokes parameters from experimental measurements under different (a) orientation settings and (b) temperatures. Theoretical reference values are $S_1/S_0 = 0.5$, $S_2/S_0 = 0.866$, and $S_3/S_0 = 0$.

We also set two combinations of $\alpha = 40°$, $\beta = 43°$, $\alpha = 16°$, and $\beta = 6°$ to verify the performance of CSP in extreme cases, the results of which are shown in [Fig. 9]. The results fluctuate slightly more, and the residual errors of S_1/S_0, S_2/S_0, and S_3/S_0 are less than 8.3×10^{-3}, 6.4×10^{-3},

Optics EXPRESS

and 8.6×10^{-3}, respectively. The residual errors of the DOP were still less than 0.5%. These results support the conclusions of the simulations described in Section 3. The experimental reconstruction errors were larger than the simulation results because of the thickness errors of the retarders, noise, and stray light.

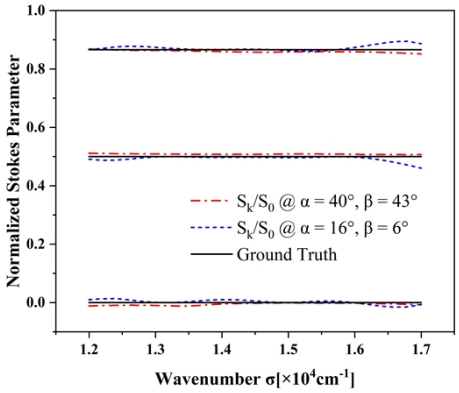

Fig. 9. Reconstructed Stokes parameters from experimental measurements. Theoretical reference values are $S_1/S_0 = 0.5$, $S_2/S_0 = 0.866$, and $S_3/S_0 = 0$.

The experimental results indicate that the CSP system can work under various orientation settings of the two retarders and is immune to the influence of temperature changes on phase retardations. This conclusion is consistent with the simulation results, indicating that the CSP system is robust and does not require effort for installation and adjustment.

5. Conclusion

In this study, we derived a general CSP model in which the orientations of the two retarders can be arbitrary and unknown. Meanwhile, the system is unaffected by environmental perturbation because it can self-calibrate to avoid fluctuations in the retarder orientations and phase retardations. We simulated the performance of the system for all possible retarder orientation combinations. The results showed that the system performed better when the fast axes of the two retarders were in the same quadrant. The fast axes of R_1 and R_2 only need to be separated by more than 2° to ensure accuracy when the fast axis of R_2 is in the range of 30°–70°. The feasibility, validity, and robustness of the proposed model were verified experimentally in the presence of temperature changes. The residual errors of the normalized Stokes parameters are of the order of 10^{-3}, and the residual error of the DOP is less than 0.5%, which meets practical application requirements. Using the proposed model, the CSP system has almost no tolerance requirements and does not require periodic recalibration, which is very beneficial for practical applications.

Funding. CIOMP-Fudan University Joint Fund (Y9R633A190); National Natural Science Foundation of China (61627819, 61727818, 6187030909, 61875192, 61805235); STS Project of the Chinese Academy of Sciences (KFJ-STS-SCYD-212, KFJ-STS-ZDTP-049, KFJ-STS-ZDTP-057).

Disclosures. The authors declare no conflicts of interest.

Data availability. Data underlying the results presented in this paper are not publicly available at this time but may be obtained from the authors upon reasonable request.

Optics EXPRESS

References

1. S. Jones, F. Iannarilli, and P. Kebabian, "Realization of quantitative-grade fieldable snapshot imaging spectropolarimeter," Opt. Express **12**(26), 6559–6573 (2004).
2. F. Snik, T. Karalidi, and C. U. Keller, "Spectral modulation for full linear polarimetry," Appl. Opt. **48**(7), 1337 (2009).
3. K. Hart, M. Kupinski, D. Wu, and R. Chipman, "First results from an uncooled LWIR polarimeter for cubesat deployment," Opt. Eng. **59**(07), 1 (2020).
4. H. M. Le, T. H. Le, Q. H. Phan, and T. T. H. Pham, "Mueller matrix imaging polarimetry technique for dengue fever detection," Opt. Commun. **502**, 127420 (2022).
5. E. Du, H. He, N. Zeng, M. Sun, Y. Guo, J. Wu, S. Liu, and H. Ma, "Mueller matrix polarimetry for differentiating characteristic features of cancerous tissues," J. Biomed. Opt. **19**(7), 076013 (2014).
6. A. Tuniyazi, T. Mu, X. Jiang, F. Han, H. Li, Q. Li, H. Gong, W. Wang, and B. Qin, "Snapshot polarized light scattering spectroscopy using spectrally-modulated polarimetry for early gastric cancer detection," J Biophotonics **14**(9), e202100140 (2021).
7. N. J. Pust and J. A. Shaw, "Wavelength dependence of the degree of polarization in cloud-free skies: simulations of real environments," Opt. Express **20**(14), 15559–5568 (2012).
8. K. Oka and T. Kato, "Spectroscopic polarimetry with a channeled spectrum," Opt. Lett. **24**(21), 1475–1477 (1999).
9. F. J. Iannarilli Jr., S. H. Jones, H. E. Scott, and P. Kebabian, "Polarimetric-spectral intensity modulation (PSIM): Enabling simultaneous hyperspectral and polarimetric imaging," Proc. SPIE 3698, 474–1477 (1999).
10. T. Mu, C. Zhang, C. Jia, W. Ren, L. Zhang, and Q. Li, "Alignment and retardance errors, and compensation of a channeled spectropolarimeter," Opt. Commun. **294**, 88–95 (2013).
11. J. Craven-Jones, B. M. Way, M. W. Kudenov, and J. A. Mercier, "Athermalized channeled spectropolarimetry using a biaxial potassium titanyl phosphate crystal," Opt. Lett. **38**(10), 1657–1659 (2013).
12. F. Snik, J. H. H. Rietjens, G. van Harten, D. M. Stam, C. U. Keller, J. M. Smit, E. C. Laan, A. L. Verlaan, R. ter Horst, R. Navarro, K. Wielinga, S. G. Moon, and R. Voors, "SPEX: the spectropolarimeter for planetary exploration," Proc. SPIE **7731**, 77311B (2010).
13. B. Cairns, E. E. Russell, J. D. LaVeigne, and P. M. Tennant, "Research scanning polarimeter and airborne usage for remote sensing of aerosols," Proc. SPIE **5158**, 33–44 (2003).
14. F. Han, T. Mu, A. Tuniyazi, D. Bao, H. Gong, Q. Li, Z. Chen, and C. Zhang, "Iterative reconstruction for snapshot intensity-modulated linear imaging spectropolarimetry without Fourier transform and phase calibration," Opt. Laser Eng. **134**, 106286 (2020).
15. F. Han, T. Mu, D. Bao, A. Tuniyazi, Q. Li, H. Gong, Z. Chen, and C. Zhang, "Iterative reconstruction for general linear imaging polarimetry without polarimetric calibration," Opt. Lett. **45**(1), 57–60 (2019).
16. B. Yang, X. Ju, C. Yan, and J. Zhang, "Alignment errors calibration for a channeled spectropolarimeter," Opt. Express **24**(25), 28923–28935 (2016).
17. X. Ju, B. Yang, J. Zhang, and C. Yan, "Reduction of the effects of angle errors for a channeled spectropolarimeter," Appl. Opt. **56**(33), 9156–9164 (2017).
18. X. Ju, B. Yang, C. Yan, J. Zhang, and W. Xing, "Easily implemented approach for the calibration of alignment and retardation errors in a channeled spectropolarimeter," Appl. Opt. **57**(29), 8600–8613 (2018).
19. D. S. Sabatke, A. M. Locke, E. L. Dereniak, and R. W. McMillan, "Linear calibration and reconstruction techniques for channeled spectropolarimetry," Opt. Express **11**(22), 2940–2952 (2003).
20. D. S. Sabatke, A. M. Locke, E. L. Dereniak, and R. W. McMillan, "Linear operator theory of channeled spectropolarimetry," J. Opt. Soc. Am. A **22**(8), 1567–1576 (2005).
21. G. Zhou, Y. Li, and K. Liu, "Efficient calibration method of total polarimetric errors in a channeled spectropolarimeter," Appl. Opt. **60**(13), 3623–3628 (2021).
22. A. Taniguchi and K. Oka, "Stabilization of a channeled spectropolarimeter by self-calibration," Opt. Lett. **31**(22), 3279–3281 (2006).
23. W. Xing, X. Ju, C. Yan, B. Yang, and J. Zhang, "Self-correction of alignment errors and retardations for a channeled spectropolarimeter," Appl. Opt. **57**(27), 7857–7864 (2018).
24. B. D. Chrysler, K. Oka, Y. Otani, and N. Hagen, "Dynamic calibration for enhancing the stability of a channeled spectropolarimeter," Appl. Opt. **59**(30), 9424–9433 (2020).
25. R. A. Chipman, "Polarimetry," in *Handbook of Optics*, M. Bass, ed. (McGraw-Hill, 1995).
26. R. J. Peralta, C. Nardell, B. Cairns, E. E. Russell, L. D. Travis, M. I. Mishchenko, and R. J. Hooker, "Aerosol polarimetry sensor for the Glory Mission," Proc. SPIE **6786**, 67865L (2007).